Supplementary Information for

The TLR2/TLR6 ligand FSL-1 mitigates radiation-induced hematopoietic injury in mice and nonhuman primates

W. June Brickey[a,b], David L. Caudell[c], Andrew N. Macintyre[d], John D. Olson[c], Yanwan Dai[e], Sirui Li[b,f], Gregory O. Dugan[c], J. Daniel Bourland[g], Lisa M. O'Donnell[c], Janet A. Tooze[h], Guannan Huang[b,f], Shuangshuang Yang[b,f], Hao Guo[b,f], Matthew N. French[d], Allison N. Schorzman[i], William C. Zamboni[i], Gregory D. Sempowski[d], Zhiguo Li[e,j], Kouros Owzar[e,j], Nelson J. Chao[k], J. Mark Cline[c], Jenny P.Y. Ting[a,b,f]

[a]Department of Microbiology and Immunology, University of North Carolina at Chapel Hill, Chapel Hill, NC, 27599

[b]Lineberger Comprehensive Cancer Center, Center of Translational Immunology, University of North Carolina at Chapel Hill, Chapel Hill, NC, 27599

[c]Department of Pathology, Section on Comparative Medicine, Wake Forest University School of Medicine, Winston Salem, NC, 27157

[d]Duke Human Vaccine Institute, Department of Medicine, Duke University School of Medicine, Durham, NC, 27710

[e]Department of Biostatistics and Bioinformatics, Duke University School of Medicine, Durham, North Carolina, 27705

[f]Department of Genetics, University of North Carolina at Chapel Hill, Chapel Hill, NC, 27599

[g]Department of Radiation Oncology, Wake Forest University School of Medicine, Winston Salem, NC, 27157

[h]Department of Biostatistics and Data Science, Wake Forest University School of Medicine, Winston Salem, NC, 27157

[i]Department of Pharmacology, University of North Carolina at Chapel Hill, Chapel Hill, NC, 27599 USA

[j]Duke Cancer Institute, [e]Department of Biostatistics and Bioinformatics, Duke University School of Medicine, Durham, North Carolina, 27705

[k]Department of Medicine, Duke University School of Medicine, Durham, NC, 27705

Supplementary Materials and Methods

Pharmacokinetics (PK)

Synthetic TLR2/TLR6 binding diacyl lipopeptide (Pam2CysGlyAspProLysHisProLysSerPhe) was obtained from Invivogen (San Diego, CA, USA), synthesized in large quantities as a VacciGrade endotoxin-free biomolecule. PK parameters were initially determined in unirradiated mice given 0.4, 0.8, or 4.0 mg/kg FSL-1 and subsequently evaluated in total body irradiated (TBI) mice given 0.8 mg/kg FSL-1. PK analysis was also performed in naïve nonhuman primates (NHP), using 0.03 or 0.09 mg/kg FSL-1 administered subcutaneously. Blood was collected in potassium-Etheylenediaminetetraacetic Acid (K_2-EDTA) vacutainers from treated NHP between 0 to 96 h following drug administration. Plasma samples were processed with 10% trifluoroacetic acid (TFA) and FSL-1 concentrations were measured using liquid chromatography-tandem mass spectrometry (Shimadzu LC-20AD liquid chromatograph Thermo TSQ Ultra triple quadrupole mass spectrometer).

Mouse CBC Analysis

To assess hematologic recovery post-radiation, blood was collected into EDTA tubes using terminal cardiac puncture of naïve mice and treated mice at days 8, 17 and 30 after radiation. Complete blood counts (CBC), including hematocrit, red blood cell (RBC) indices, total and differential leukocyte, hemoglobin, and platelet counts were determined using standard animal hematological testing using IDEXX ProCyte Dx™ Hematology Analyzer as conducted at Animal Clinical Laboratory Services, University of North Carolina at Chapel Hill.

Mouse Bone Marrow Cell Immunophenotyping

Bone marrow (BM) cells flushed from femurs were treated with ammonium chloride-potassium lysing buffer (Lonza) to lyse red blood cells. BM cells were stained for viability with live/dead fix aqua (Invitrogen) and then all cells were labelled for 30 min at 4°C with fluorescently tagged antibodies in phosphate-buffered saline (PBS) with 1% bovine serum albumin (BSA) (Invitrogen). Labelled cells were fixed using 4% paraformaldehyde (ThermoFisher). Fixed cells were stained at room temperature (RT) with 3 μM (4′,6-diamidino-2-phenylindole) (DAPI) in permeabilization buffer (Biolegend) and then all cells were analyzed using an LSRII flow cytometer (BD Biosciences), operating with Diva software v8.0 (BD Biosciences). The resultant data were gated

using FlowJo software v10.4 (BD Biosciences). Cell targets, clones, fluorophores, and suppliers are listed in ***SI Appendix*, Table S1**. BM cell populations were defined as follows: common myeloid progenitors (CMP): Lineage or Lin$^-$ (CD3ε, CD11b, B220, TER-119, Ly-6G/Ly-6C) Sca1$^-$ c-kit$^+$ CD16/32^{int}; granulocyte-macrophage progenitors (GMP): Lin$^-$ Sca1$^-$ c-kit$^+$ CD16/32^{hi}; megakaryocyte-erythrocyte progenitors (MEP): Lin$^-$ Sca1$^-$ c-kit$^+$ CD16/32^{low}; hematopoietic stem progenitor cells (HSPC): Lin$^-$ Sca1$^+$ c-kit$^+$ (1); eosinophils: Gr1$^-$ CD115^{low} F4/80$^+$ SSC^{high}, macrophages: Gr1$^-$ CD115^{low} F4/80$^+$SSC$^{low/mid}$ (2); erythroid: Ter119$^+$; B cells and B cell progenitors: B220$^+$ and T cells: CD3$^+$. Representative gating strategies are shown in ***SI Appendix* Fig. S2A-B**.

NHP Protein Multiplex Bead Array Analysis

Cryopreserved NHP plasma was thawed and assayed using a premixed 23-plex magnetic bead panel for G-CSF, GM-CSF, IFN-γ, IL-1ra, IL-1β, IL-2, IL-4, IL-5, IL-6, IL-8, IL-10, IL-12/23 (p40), IL-13, IL-15, IL-17, IL-18, MCP-1, MIP-1α, MIP-1β, sCD40L, TGF-α, TNF and VEGF (Millipore). The assay was prepared according to the manufacturer's protocol and read using a Bio-Plex 3D bead reader (Bio-Rad). Data were analyzed using Bio-Plex manager software v6.2 (Bio-Rad) and visualized in heatmaps in ***SI Appendix,* Fig. S5**.

NHP PBMC Immunophenotyping

Monkeys were sedated with intramuscular ketamine and then femoral blood was drawn into sodium- or lithium-heparin coated collection tubes (BD Bioscience), transferred by courier to Duke University and stored overnight at RT. The next day, plasma and peripheral blood monocytic cells (PBMC) were isolated using System-Histopaque-1077 media according to the manufacturer's protocol (Sigma-Aldrich). Peripheral blood monocytic cells (PBMC) were immunophenotyped on the day of isolation and plasma was cryopreserved for later use. PBMC were labelled for 40 min at room temperature (RT) with fluorescently tagged antibodies in PBS with 1% BSA, stained for viability using live/dead fix aqua (Invitrogen) and then fixed in 4% paraformaldehyde (ThermoFisher). Fixed cells were analyzed as described for mouse cells. Cell targets, clones, fluorophores, and suppliers are listed in ***SI Appendix*, Table S1**. Plasmacytoid and myeloid DC were defined as CD3$^-$ CD20$^-$ HLA-DR$^+$ CD14$^-$ CD123$^+$ CD11c$^-$ and CD3$^-$ CD20$^-$ HLA-DR$^+$ CD14$^-$ CD123$^-$ CD11c$^+$, respectively (3). B cells

were defined as $CD45^+$ $CD20^+$; T cells as $CD45^+$ $CD3^+$ $CD16^-$ and NK-T cells as $CD45^+$ $CD3^+$ $CD16^+$. Activated monocytes were defined as $CD45^+$ $CD3^-$ $CD20^-$, HLA-DR^+/$CD14^+$, $CD16^+$ $CD14^{+/low}$ and classic monocytes as $CD45^+$ $CD3^-$ $CD20^-$, HLA-DR^+/$CD14^+$, $CD16^-$ $CD14^+$ (4). Representative gating strategies are shown in ***SI Appendix*, Fig. S6A-B**.

Immunoblotting of mouse bone marrow protein lysates

Mouse BM protein lysates were prepared in radio-immunoprecipitation assay (RIPA) lysis buffer (Thermo Fisher), supplemented with protease and phosphatase inhibitors (Roche). The lysates were analyzed by immunoblotting after electrophoresis on 4–12% NuPAGE Bis-Tris polyacrylamide gels (Thermo Fisher) and transferred to nitrocellulose membranes (Bio-Rad). For detection, the following antibodies were used: phosphorylated p38 (#4511), p38 (#9212), phosphorylated H2AX (#9718) (Cell Signaling); Goat anti-rabbit-HRP (#111-035-144, Jackson Immune Research Laboratories) and β-actin-horse radish peroxidase (HRP) conjugate (#47778, Santa Cruz Biotechnology). Protein bands on probed membranes were quantified using ImageJ (NIH public domain). The blot and density quantitation are presented in ***SI Appendix*, Fig. S7**.

Statistical Analyses

Data points failing the outlier calculator based on the Grubbs' test or extreme studentized deviate method (5) by GraphPad Prism (version 9) with alpha significance at 0.05 were considered outliers and were removed from the raw data files before any statistical tests were conducted. This affected the following figures: Fig 1 I-L, Fig 2G, Fig 4B-C, Fig S2C-J, Fig S4A, and Fig S7C. All subsequent analyses unless noted otherwise below were conducted using the R statistical environment (6) (version 4.2.2), along with extension packages from the Comprehensive R Archive Network (CRAN).

The association of treatment with overall survival was evaluated. Differences between survival distributions were illustrated in Kaplan-Meier plots and log-rank test was conducted using the SURVIVAL package (7) (version 3.2-13). The Log-rank test *P* values are reported. Power calculations were conducted to determine the minimum detectable effect size for a two-sample Wilcoxon test. The calculations assumed 10 NHP in each of the two treatment groups and quantified the effect as the ratio of the difference of the two

means divided by a common standard deviation. For an unadjusted two-sided alpha level of 0.05, we found 0.8 power to detect an effect size of 1.42.

Differences in the distributions of continuous outcomes or calculated changes in outcomes over a period of time among treatment, radiation or genotype groups were evaluated using the two-sample *t* test for unpaired data with Welch's approximation (8). When the assumption of normality was not deemed to be appropriate based on the measurements' distributions, the Wilcoxon rank sum test was applied to unpaired data and asymptotic *P* values were reported (9). To evaluate simultaneously the effect of multiple grouping variables (treatment x radiation or genotype x treatment x radiation) on the outcomes, two-way or three-way ANOVA tests with interaction terms were applied with the function aov from STATS package in R (10).

Repeated measurements data were modeled using linear mixed-effects models implemented by the LME4 package (11) (version 1.1-31). In some cases, the fitted linear mixed-effects model was singular, so Bayesian linear mixed-effects model implemented by the BLME package (12) (version 1.0-5) was applied instead. In cases where the number of pre-treatment days were reported for baseline values or no baseline values were available, the postulated regression model included additive fixed effects for time and treatment, along with their pairwise interaction were reported. For variables where indicated baseline was categorical, the regression model was augmented by including a fixed additive effect for the baseline value along with first- and second-order interaction terms unless otherwise specified. In cases where the outcomes over time did not follow a linear pattern and the data were measured at more than four time points, the turning point of the measurement for each sample was detected according to Kendall's information theory (implemented by the function turnpoint from PASTECS package, version 1.3.21) (13, 14) (***SI Appendix,* Fig. S3A-E and S4G-L**); the turning point was determined via a majority vote (except where a common turning point was selected to keep consistency in related measurements, ***SI Appendix,* Fig. S4I**). Then, we separated the data at the determined turning point and aligned two mixed-effects models before (pre) and after (post) the turning point, where the model after the turning point included the turning point and the pre-turning point model included the baseline as a fixed additive effect. In cases where the outcomes over time did not follow a linear pattern and the data was measured at less than or equal to four time points, the mixed-effects model was fit for the entire timeline, but the time was treated as discrete unordered factors instead of a continuous variable. If the baseline

existed, it was either treated as a fixed additive effect (***SI Appendix,* Fig. S3J**) or merged into time as the base factor (***SI Appendix,* Fig. S5**) depending on how the *P* values were reported. To ensure that model residuals did not violate the normality assumption, the Box-Cox power transformation (15) was applied to each outcome prior to each linear mixed-effects analysis. The Box-Cox power used in the transformation was estimated from a fixed effects linear model with the same formula as mixed-effects modeling (excluding the random effects). A constant (1) was added to all values of the data panels with 0 values before transformation. The Box-Cox power estimation was implemented by the MASS package (16) (version 7.3-58.1). In cases where variables were on different scales, rescaling was applied with the function scale from BASE package (i.e., on time, if time was treated as numerical values; on baseline, if baseline was applicable). If the time was treated as continuous or if the time was treated as discrete factors but the baseline was included as a fixed additive effect, the effect of each term in the mixed-effects model at all levels was estimated using the sum of squares for each term (including the interaction term). The F test with Type III sums of squares (17) was implemented by the CAR package (18) (version 3.1.1) and generated *P* values. On the other hand, if time was treated as a discrete factor and the baseline was treated as the base factor merged into the time effect instead of as a fixed additive effect, the *P* values were estimated for each term by t-statistics using Satterthwaite's method implemented by the LMERTEST package (19) (version 3.1-3).

The ordinal logistic regression, implemented by the MASS package (16) (version 7.3-58.1), was applied to analyze the effect of treatment on bruising over time (**Fig. 2K**). The ordinal logistic regression model included additive fixed effects for time and treatment along with their pairwise interaction.

Inference on NHP BM progenitor cell abundance was conducted using Fisher's exact test with the raw data (20). For **Fig. 3G-K**, changes of abundance of cell types (ordinal data) from baseline to day 22, day 22 to day 65 and baseline to day 65 were calculated. Contingency tables were inferred from the abundance changes, which were based on the Fisher's exact test for FSL-1 vs. Vehicle.

NanoString nCounter RNA sequencing counts were generated for 24 genes, along with positive and negative controls (***SI Appendix*, Table S2**). Normalization was performed based on well-correlated (Pearson correlation coefficient >0.8) positive controls, followed by background correction using the negative controls. Specifically, geometric means of the four positive controls were calculated within each sample, then the

average of the geometric means across samples was taken. For each sample, the normalization factor was calculated as the overall average divided by the geometric mean for that sample, and the counts for each gene in the sample were multiplied by this normalization factor. Next, normalized counts for each gene were divided by the geometric mean of all eight negative controls for that sample. For the analysis, $\log_2$ transformed ratios of the preprocessed counts for day 22 vs. baseline, day 65 vs. baseline, and day 65 vs. day 22 were identified for each gene. Then, differences in $\log_2$ transformed ratios among treatment groups were compared using the two-sample *t* test for unpaired data. Pooled variance was used to estimate the variance in the testing results (8, 21). Both un-adjusted *P* values and *P* values adjusted for multiple testing (false discovery rate) (22) are reported in ***SI Appendix,* Table S2**.

Supplementary Figure S1.

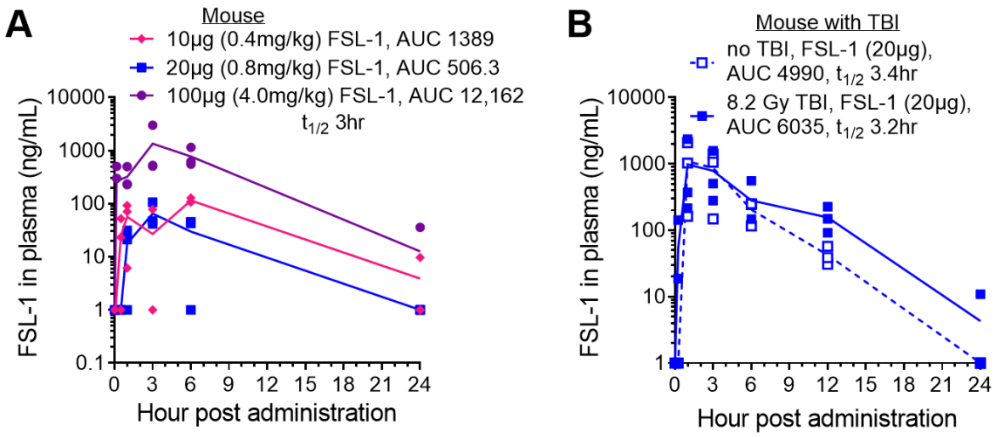

Fig. S1. Pharmacokinetics of FSL-1 subcutaneous administration in mice was evaluated.

Pharmacokinetics was evaluated in non-irradiated **(A)** and irradiated **(B)** C57BL/6 mice using 10 to 100 mg FSL-1 administered sc and blood collected over 72 h. Detectable FSL-1 in plasma for the initial 24 h was assayed by LC-MS/MS, with Area Under Curve (AUC) values and half-life ($t_{1/2}$) indicated. Each symbol represents an individual mouse.

Supplementary Figure S2.

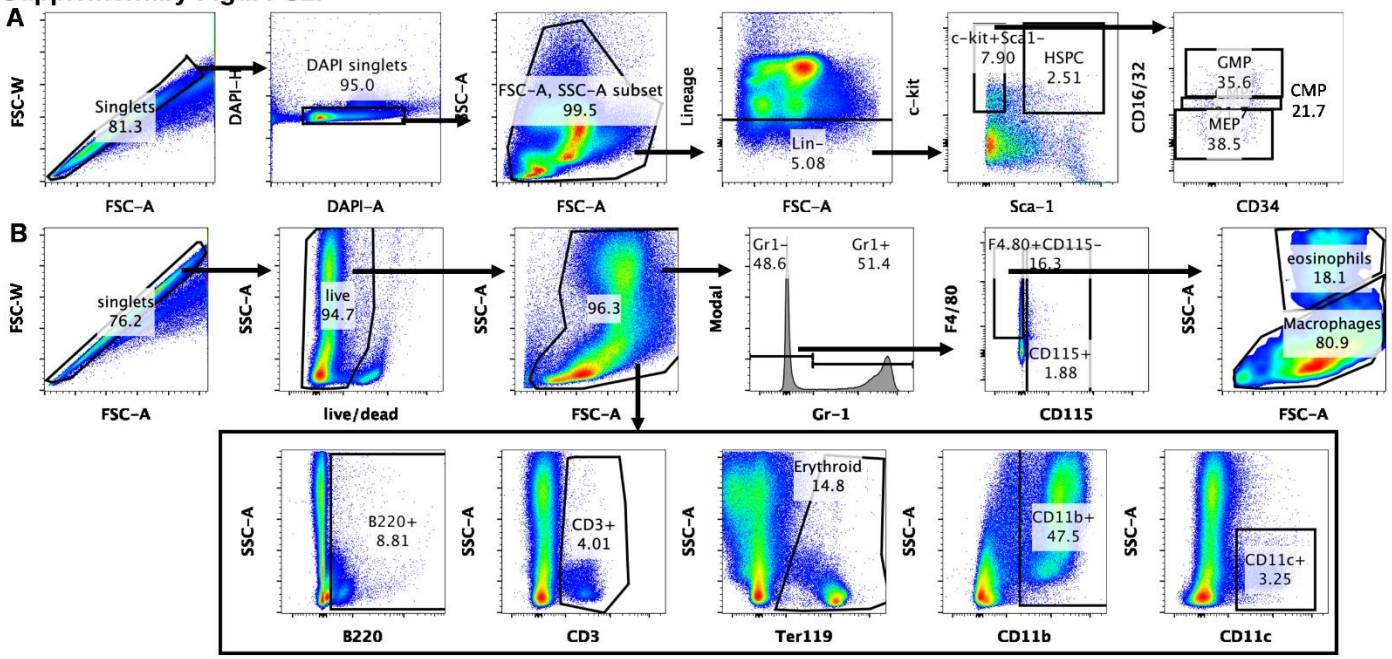

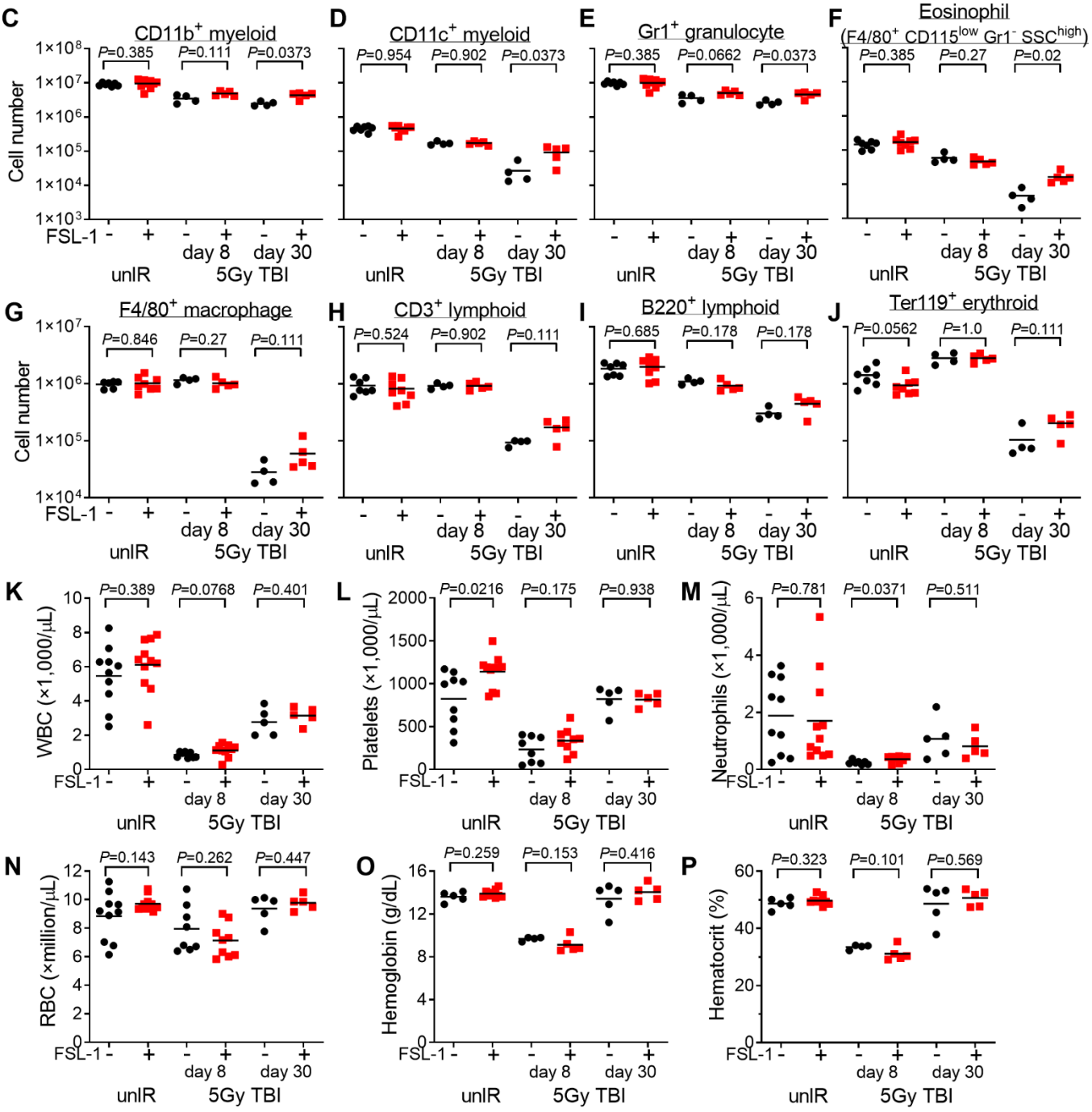

Fig. S2. FSL-1 administration impacted maturing myeloid cell lineages in bone marrow and neutrophils in peripheral blood of treated mice.

Bone marrow (BM) cells were isolated from C57BL/6 mice and immunophenotyped by flow cytometry. Control mice were unirradiated (unIR), whereas experimental mice were exposed to 5 Gy total body irradiation (TBI). Mice received sc injections of PBS (-) or FSL-1 (+) on day 1 with BM samples harvested for immunophenotyping on days 8 or 30. **(A)** Flow gating strategy for BM progenitor cells. **(B)** Flow gating strategy for maturing lineages. **(C)** CD11b$^+$ myeloid cells, **(D)** CD11c$^+$ myeloid cells, **(E)** Gr1$^+$ granulocytes, **(F)**

eosinophils, **(G)** F4/80^{+} macrophage, **(H)** CD3^{+} cells, **(I)** B220^{+} cells and **(J)** Ter119^{+} erythroid cells in BM cell suspensions were quantified. Each symbol represents an individual and the bar signifies the mean. Unpaired Wilcoxon rank sum tests between PBS and FSL-1 treatments were applied to determine differences in cell numbers with *P* values shown. Blood cells were measured in peripheral blood samples taken from treated mice on days 8 and 30 after radiation. The constituents include white blood cells, WBC **(K)**, platelets **(L)**, neutrophils **(M)**, red blood cells, RBC **(N)**, hemoglobin **(O)** and hematocrit **(P)**. An unpaired *t* test (two-sided, equal variance) was applied to compare PBS and FSL-1 values at each time point with *P* values displayed. Each symbol represents an individual mouse with bar at mean.

Supplementary Figure S3.

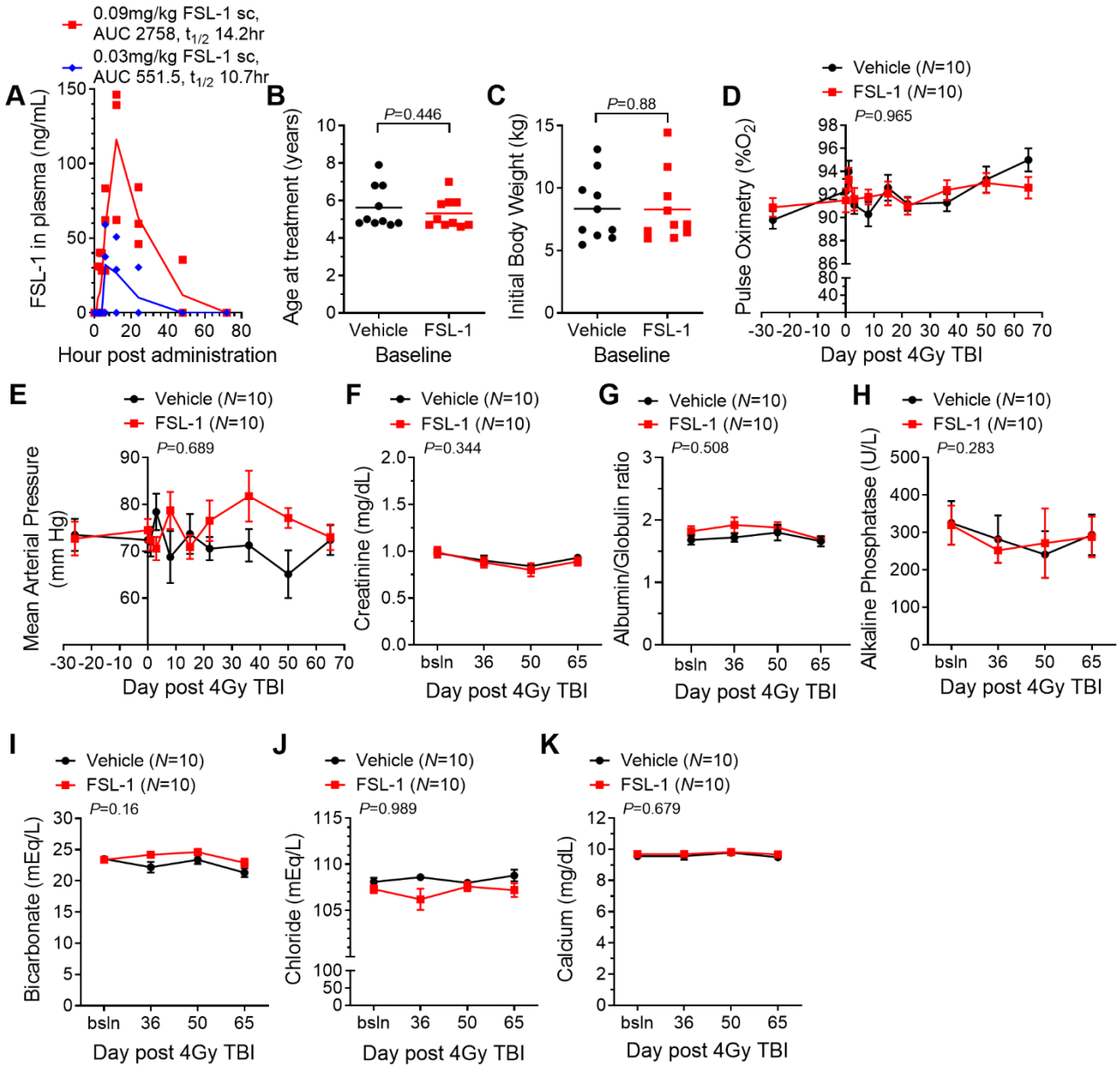

Fig. S3. Administration of FSL-1 in NHP after exposure to sublethal TBI did not cause adverse effects. **(A)** Pharmacokinetics testing was conducted in non-irradiated NHP using either 0.03 or 0.09 mg/kg FSL-1 sc with blood collected over 3 d after FSL-1 administration (*N* = 3 per cohort, indicated by symbols). The AUC of FSL-1 in plasma and the half-life ($t_{1/2}$) are shown. To evaluate FSL-1 mitigation of H-ARS in NHP, a sublethal TBI (4 Gy) model was used, followed with subcutaneous FSL-1 administration at 24 h after radiation. **(B)** Initial age and **(C)** body weight of NHP; each symbol represents an individual and the bar signifies the mean. Wilcoxon rank sum tests were performed to discern statistical differences, with indicated *P* values. Physiologic

measures of **(D)** pulse oximetry and **(E)** mean arterial pressure were analyzed. Blood chemistry markers of **(F)** Creatinine, **(G)** Albumin/Globulin ratio, **(H)** Alkaline Phosphatase, **(I)** Bicarbonate, **(J)** Chloride and **(K)** Calcium in peripheral blood (PB) samples were assessed. For **D-K**, outcomes are represented by mean +/- SEM for *N* = 10 per treatment cohort. A linear mixed-effects model was used to examine the impact of FSL-1 vs. Vehicle treatment over time, with *P* values shown for treatment interaction with time.

Supplementary Figure S4.

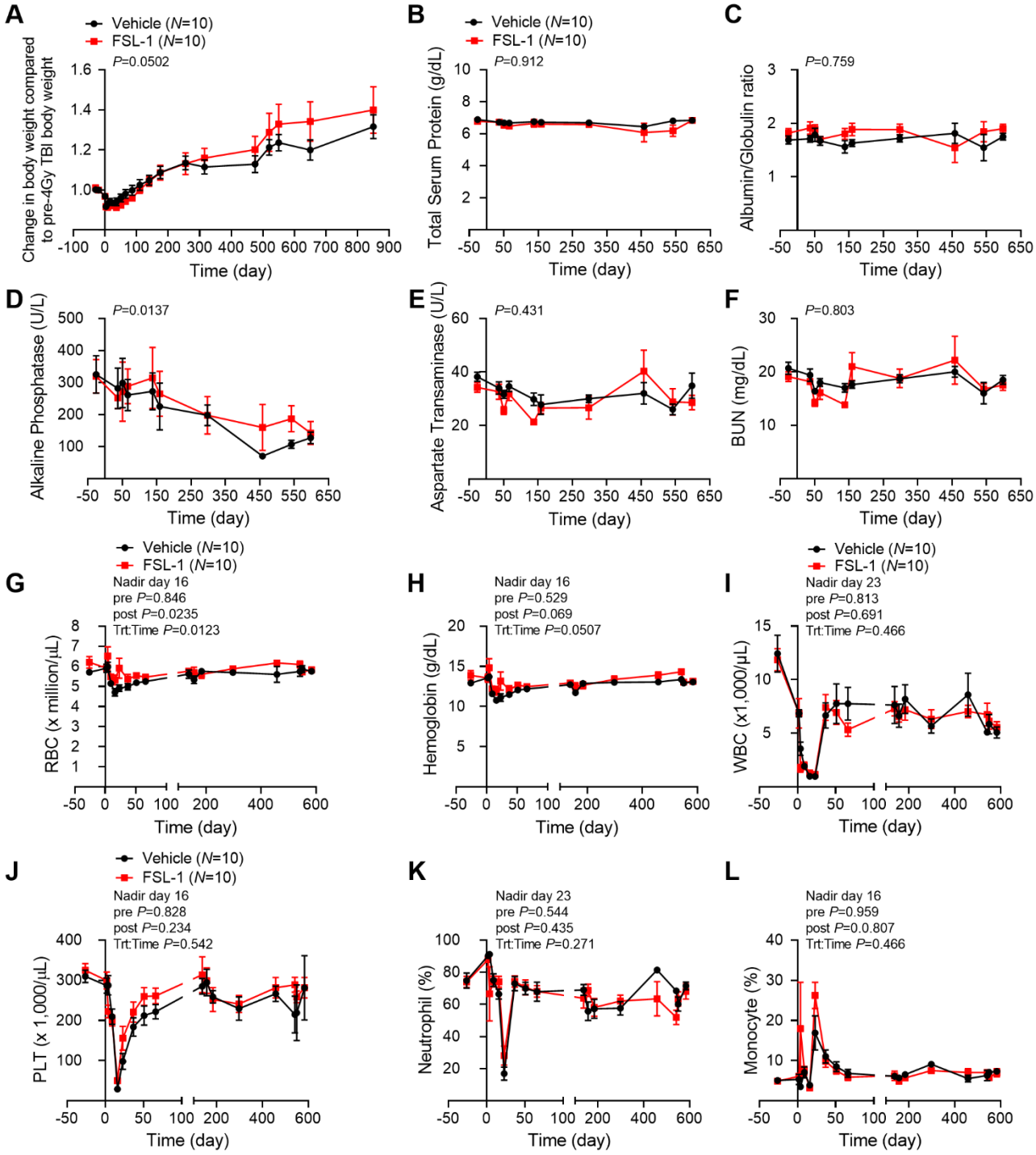

Fig. S4. Chronic weight, clinical or hematologic deficits were not evident with FSL-1 administration after radiation in NHP.

NHP were monitored after the 65-d study period for up to 850 d. **(A)** Body weight as a fraction of baseline body weight. Clinical metrics for **(B)** Total Serum Protein, **(C)** Albumin/Globulin ratio, **(D)** Alkaline Phosphatase, **(E)**

Aspartate Transaminase, and **(F)** Blood Urea Nitrogen, BUN were assessed. Hematologic markers in complete blood counts of **(G)** red blood cells, RBC, **(H)** Hemoglobin, **(I)** white blood cells, WBC, **(J)** platelets, PLT, **(K)** Neutrophils, and **(L)** Monocytes were determined. Data points are expressed as mean +/- SEM, for *N* = 10 per cohort with *P* values for treatment interaction with time determined by linear mixed-effects model analyses. For **G-L**, the nadir with linear mixed-effects model was applied pre and post nadir to analyze differences in injury and recovery profiles. *P* values for treatment pre or post nadir and treatment to time interaction (Trt:Time) are shown.

Supplementary Figure S5.

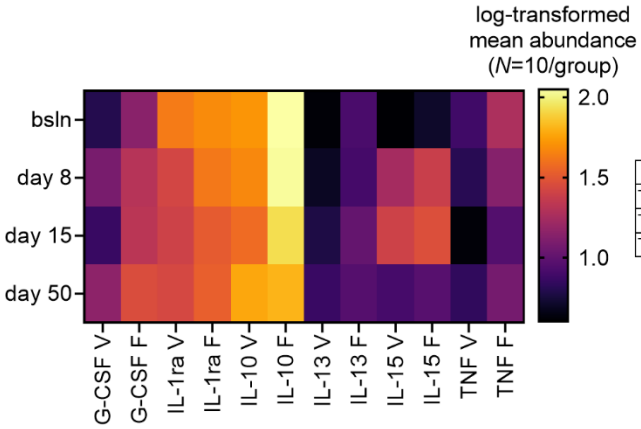

	G-CSF	IL-1ra	IL-10	IL-13	IL-15	TNF
Trt:Time d8	0.600	0.200	0.842	0.570	0.355	0.782
Trt:Time d15	0.932	0.499	0.329	0.713	0.884	0.737
Trt:Time d50	0.973	0.592	0.471	0.898	0.918	0.722

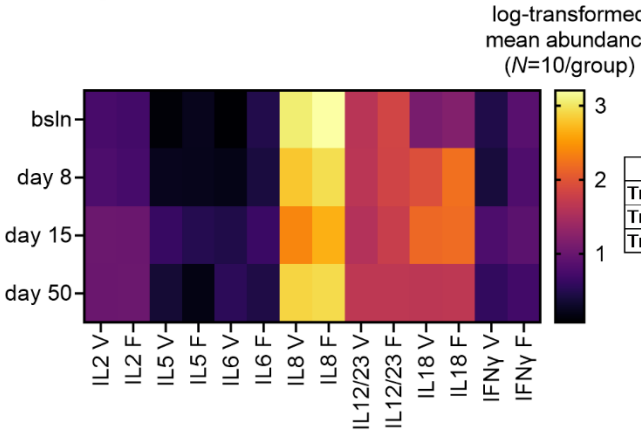

	IL-2	IL-5	IL-6	IL-8	IL-12/23	IL-18	IFNγ
Trt:Time d8	0.344	0.716	0.720	0.316	0.912	0.315	0.064
Trt:Time d15	0.955	0.718	0.260	0.810	0.823	0.506	0.382
Trt:Time d50	0.861	0.398	0.412	0.064	0.316	0.565	0.580

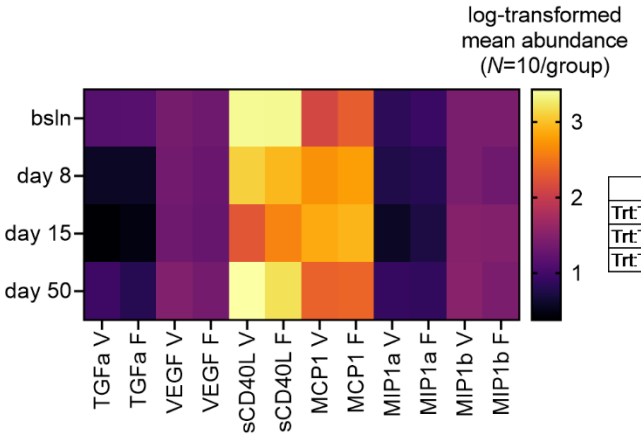

	TGFa	VEGF	sCD40L	MCP1	MIP1a	MIP1b
Trt:Time d8	0.708	0.371	0.221	0.454	0.717	0.494
Trt:Time d15	0.995	0.575	0.109	0.139	0.079	0.847
Trt:Time d50	0.553	0.158	0.087	0.057	0.698	0.293

Fig. S5. Minimal changes were observed in serum proteins of NHP treated with radiation plus FSL-1. Serum cytokines were measured by multiplex bead array. Heat maps show mean log transformed abundance (pg/mL) of each analyte for plasma from Vehicle-(V) and FSL-1-(F)treated samples at baseline and on days 8, 15 and 50. The *P* values determined by linear mixed-effects model indicate treatment with time interactions, where treatment or Trt is Vehicle vs. FSL-1 and time periods or Time are baseline (bsln) vs. days (d) 8, 15 or 50.

Supplementary Figure S6.

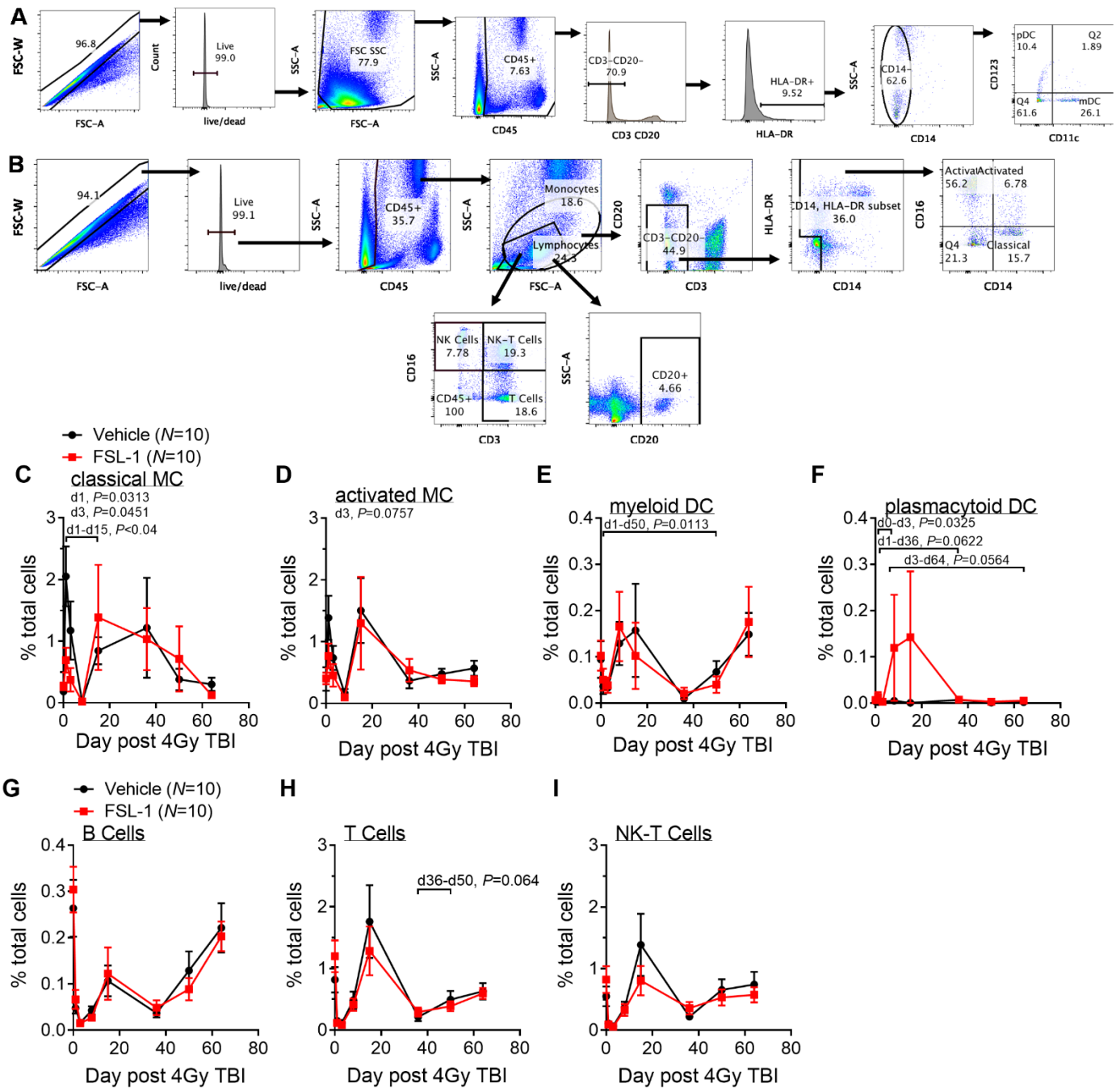

Fig. S6. Alterations were found in myeloid cells in peripheral blood of treated NHP.

Peripheral blood (PB) was collected at baseline and selected times for up to 65 d after radiation of treated NHP. **(A)** Flow cytometry gating strategy for dendritic cells (DC). **(B)** Flow cytometry gating strategy for monocytes and lymphocytes. **(C)** Classical monocytes (MC) and **(D)** activated MC were monitored in PB samples. **(E)** Myeloid DC (mDC) and **(F)** plasmacytoid DC (pDC) were quantified. Lymphocyte populations of

(G) B cells, **(H)** T cells and **(I)** NK-T cells were measured. Data is presented as mean +/- SEM for *N* = 10 for each cohort. Statistical differences between Vehicle and FSL-1 treatments were evaluated using Wilcoxon rank sum testing at each time point and each time bracket, with selected *P* values shown. The brackets span the time points of comparisons.

Supplementary Figure S7.

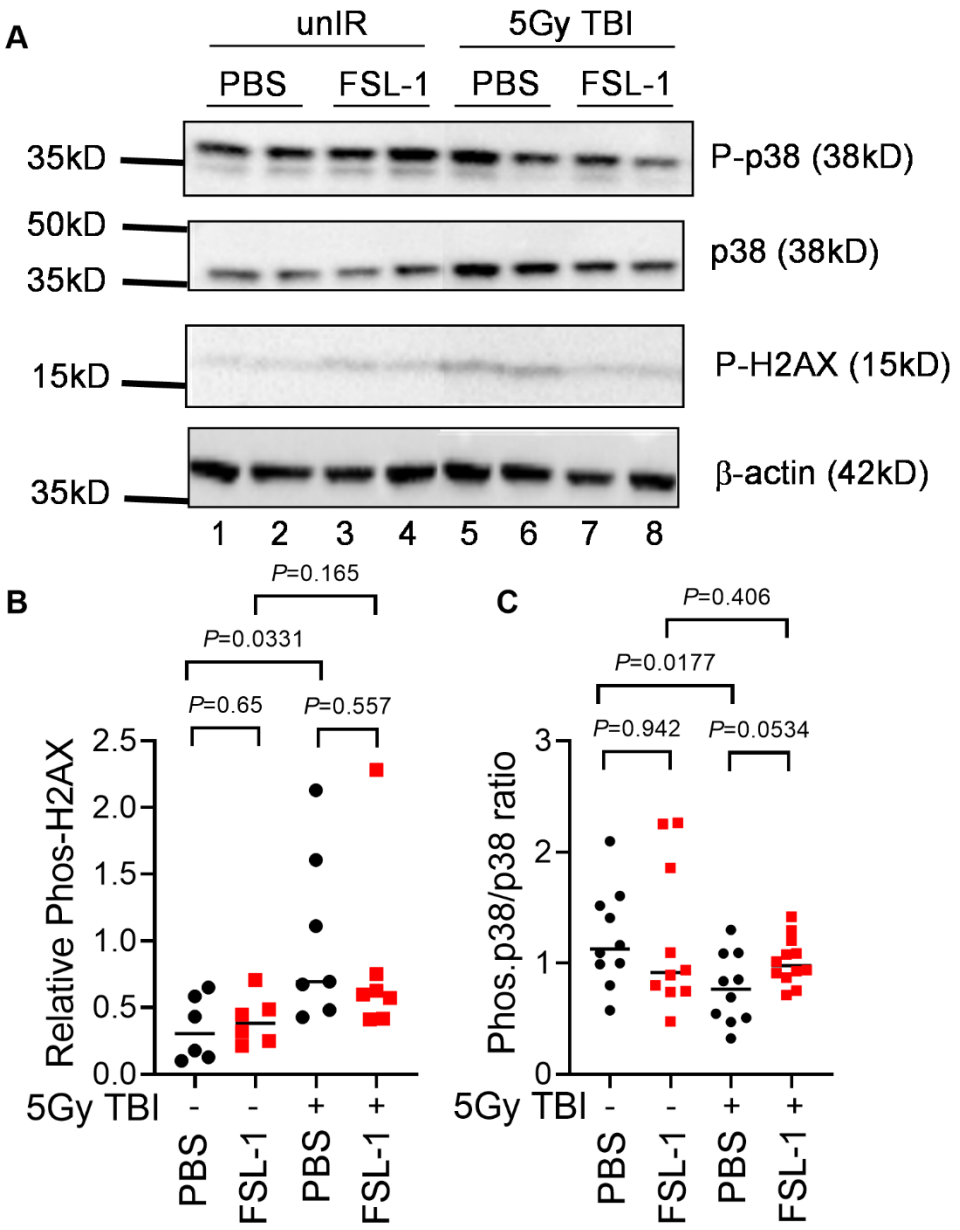

Fig. S7. Radiation, but not FSL-1, impacted MAPK p38 phosphorylation and a damage marker. (A) The abundance of phosphorylated (Phos or P-) and total p38, phosphorylated H2AX and β-actin proteins in bone marrow cell lysates prepared from C57BL/6 mice necropsied on day 8 after radiation were examined by immunoblotting, with a representative blot shown. **(B)** Quantitation of relative levels of phosphorylated H2AX to β-actin. **(C)** Quantitation of phosphorylated P-p38 and total p38 proteins detected by immunoblotting of bone marrow cell lysates prepared from unirradiated (unIR) and irradiated (5 Gy TBI) +/- FSL-1-treated WT mice. The ratio of P-p38 to total p38 protein for each target on the immunoblots was quantified using ImageJ. Each

symbol is an individual biological sample. Data were evaluated for treatment differences using a pairwise *t* test, with *P* values shown.

Table S1. Reagents used for flow cytometry immunophenotyping of mouse and NHP cell populations.			
Target	**Fluorophore**	**Clone**	**Supplier**
(A) Mouse Bone Marrow stain 1: CMP, GMP, MEP, HSPC progenitors			
Lineage Cocktail (Lin): CD3ε, CD11b, CD45R (B220), TER-119 Ly-6G/Ly-6C	PerCP-Cy5.5	145-2C11, M1/70, RA3-6B2, TER-119 RB6-8C5	BD Biosciences
Ly-6A/Ly-6E	PE	E13-161.7	BD Biosciences
CD117	FITC	2B8	BD Biosciences
CD34	APC	HM34	BioLegend
CD16/32	PE-Cy7	93	BioLegend
(B) Mouse Bone Marrow stain 2: granulocytes, macrophages, lymphocytes			
CD3ε	FITC	500A2	BioLegend
CD45R (B220)	APC-Cy7	RA3-6B2	BD Biosciences
TER-119	Brilliant Violet 711	TER-119	BD Biosciences
Gr1 (Ly-6G/Ly-6C)	PE-Cy5	RB6-8C5	BioLegend
F4/80	PE	BM8	BioLegend
CD115 (CSF-1R)	APC	AFS98	BioLegend
CD11c	Brilliant Violet 421	N418	BioLegend
CD11b	Brilliant Violet 605	M1/70	BioLegend
Flt-3	PE-Vio770	A2F10	Miltenyi Biotec
(C) NHP PBMC: dendritic cells			
CD3	APC	10D12	Miltenyi Biotec
CD20	APC	2H7	BD Biosciences
CD1c	FITC	L161	BioLegend
CD14	Brilliant Violet 711	MφP9	BD Biosciences
CD11c	PE	3.9	BioLegend
CD123	PE-Cy7	7G3	BD Biosciences
HLA-DR	APC-H7	G46-6	BD Biosciences
CD45	Brilliant Violet 605	D058-1283	BD Biosciences
(D) NHP PBMC: monocytes and lymphocytes			
CD56	FITC	B159	BD Biosciences
HLA-DR	PerCP-Cy5.5	G46-6	BD Biosciences
CD16	PE	3G8	BD Biosciences
CD8a	PE-Cy7	SK1	BioLegend
CD3	APC	10D12	Miltenyi Biotec
CD20	APC-H7	2H7	BD Biosciences
CD45	Brilliant Violet 605	D058-1283	BD Biosciences
CD14	Brilliant Violet 711	MφP9	BD Biosciences

Table S2. Differentially expressed genes in NHP BM cells with 4Gy TBI +/- FSL-1 treatment.									
Test Value	**Gene Name**	**Log_2 Fold Change**	***P* value**	**adjusted *P* value**	**tstat**	**df**	**LCI 0.95**	**UCI 0.95**	**stderr**
(A) Baseline to Day 22 comparison									
log2D22_B	*AP-1*	0.0987	0.8145	0.8886	0.2451	6	-2.0235	2.4741	0.9190
log2D22_B	*CASP3*	0.5940	0.3708	0.6728	0.9673	6	-1.0631	2.4531	0.7185
log2D22_B	*GCSF*	-0.4165	0.5447	0.7553	-0.6418	6	-2.5142	1.4693	0.8140
log2D22_B	*GM-CSF*	-0.5012	0.9462	0.9462	-0.0703	6	-2.6063	2.4606	1.0354
log2D22_B	*HDAC3*	0.1641	0.6066	0.7553	0.5431	6	-1.3357	2.0978	0.7016
log2D22_B	*IL12a*	1.4042	0.1187	0.5747	1.8198	6	-0.5065	3.4461	0.8077
log2D22_B	*IL6*	-0.4942	0.6186	0.7553	-0.5247	6	-4.2154	2.7267	1.4185
log2D22_B	*IRAK4*	0.4736	0.1844	0.5747	1.4997	6	-0.4059	1.6911	0.4285
log2D22_B	*JNK1*	0.2680	0.4811	0.7216	0.7510	6	-0.8257	1.5569	0.4869
log2D22_B	*KI67*	-1.2844	0.4662	0.7216	-0.7778	6	-3.5241	1.8241	1.0928
log2D22_B	*MMP9*	3.3628	0.1731	0.5747	1.5459	6	-1.7646	7.8195	1.9584
log2D22_B	*MyD88*	2.2549	0.0579	0.4635	2.3388	6	-0.0867	3.8413	0.8026
log2D22_B	*NEMO*	-0.3795	0.6294	0.7553	-0.5082	6	-1.5375	1.0087	0.5203
log2D22_B	*OAZ1*	1.1735	0.2155	0.5747	1.3844	6	-0.8053	2.9040	0.7579
log2D22_B	*p38 (MAPK14)*	1.3496	0.3925	0.6728	0.9212	6	-1.2860	2.8391	0.8429
log2D22_B	*P50*	0.6082	0.2151	0.5747	1.3858	6	-0.5629	2.0332	0.5305
log2D22_B	*p65 (RELA)*	0.4263	0.3865	0.6728	0.9337	6	-0.7837	1.7508	0.5179
log2D22_B	*POLR2A*	0.3792	0.3701	0.6728	0.9688	6	-0.7775	1.7968	0.5260
log2D22_B	*SDHA*	-0.0477	0.7309	0.8353	0.3605	6	-1.2418	1.6709	0.5952
log2D22_B	*TLR2*	2.4696	0.0074	0.1781	3.9634	6	1.0143	4.2873	0.6688
log2D22_B	*TLR6*	1.5113	0.0471	0.4635	2.4904	6	0.0252	2.8642	0.5801
log2D22_B	*TNF*	1.3925	0.1754	0.5747	1.5360	6	-0.7217	3.1556	0.7923
log2D22_B	*TRAF6*	-0.3261	0.8858	0.9243	-0.1499	6	-1.2951	1.1456	0.4987
log2D22_B	*UBB*	0.4412	0.2829	0.6728	1.1794	6	-0.5830	1.6680	0.4600
(B) Day 22 to Day 65 comparison									
log2D65_D22	*AP-1*	-0.7092	0.4134	0.6201	-0.8787	6	-2.7059	1.2760	0.8137
log2D65_D22	*CASP3*	-1.8148	0.0331	0.1988	-2.7536	6	-3.2781	-0.1933	0.6303
log2D65_D22	*GCSF*	-0.1746	0.7394	0.8354	-0.3485	6	-1.6816	1.2624	0.6016
log2D65_D22	*GM-CSF*	-0.0023	0.8713	0.8713	0.1690	6	-1.8103	2.0789	0.7947
log2D65_D22	*HDAC3*	-1.1215	0.5161	0.6882	-0.6897	6	-2.5127	1.4077	0.8011
log2D65_D22	*IL12a*	-1.2883	0.3086	0.5290	-1.1124	6	-2.6428	0.9909	0.7425
log2D65_D22	*IL6*	-1.6181	0.5530	0.6985	-0.6283	6	-4.5586	2.6959	1.4824
log2D65_D22	*IRAK4*	-1.7302	0.1295	0.3108	-1.7567	6	-3.0432	0.4997	0.7239
log2D65_D22	*JNK1*	-1.5986	0.2159	0.4459	-1.3830	6	-2.9865	0.8296	0.7798
log2D65_D22	*KI67*	-0.3646	0.6573	0.7888	0.4665	6	-2.8993	4.2652	1.4640
log2D65_D22	*MMP9*	-3.9975	0.0841	0.2242	-2.0682	6	-7.5308	0.6316	1.6679
log2D65_D22	*MyD88*	-2.3972	0.0197	0.1573	-3.1560	6	-4.6137	-0.5839	0.8234
log2D65_D22	*NEMO*	-0.6482	0.8370	0.8713	-0.2149	6	-2.5045	2.1002	0.9409
log2D65_D22	*OAZ1*	-1.8224	0.0676	0.2242	-2.2262	6	-3.3044	0.1561	0.7071

log2D65_D22	*p38 (MAPK14)*	-1.9485	0.0748	0.2242	-2.1529	6	-3.8768	0.2478	0.8428
log2D65_D22	*P50*	-1.8182	0.0597	0.2242	-2.3175	6	-3.1610	0.0859	0.6635
log2D65_D22	*p65 (RELA)*	-1.1974	0.3453	0.5525	-1.0240	6	-2.5010	1.0253	0.7206
log2D65_D22	*POLR2A*	-1.2835	0.2229	0.4459	-1.3593	6	-2.5314	0.7234	0.6651
log2D65_D22	*SDHA*	-1.0756	0.4647	0.6560	-0.7807	6	-2.4056	1.2419	0.7453
log2D65_D22	*TLR2*	-3.7045	0.0025	0.0510	-4.9826	6	-5.3536	-1.8272	0.7206
log2D65_D22	*TLR6*	-2.7165	0.0042	0.0510	-4.4673	6	-4.1023	-1.1987	0.5933
log2D65_D22	*TNF*	-2.5910	0.0515	0.2242	-2.4253	6	-4.6198	0.0205	0.9482
log2D65_D22	*TRAF6*	-0.8709	0.2652	0.4896	-1.2287	6	-1.9760	0.6549	0.5376
log2D65_D22	*UBB*	-0.6877	0.7658	0.8354	-0.3118	6	-2.0257	1.5678	0.7343
(C) Baseline to Day 65 comparison									
log2D65_B	*AP-1*	-1.0428	0.5636	0.7695	-0.6110	6	-2.4505	1.4712	0.8014
log2D65_B	*CASP3*	-1.1197	0.0367	0.2200	-2.6775	6	-1.9918	-0.0896	0.3887
log2D65_B	*GCSF*	-0.9602	0.2175	0.5182	-1.3776	6	-2.0324	0.5683	0.5314
log2D65_B	*GM-CSF*	-0.3764	0.9365	0.9365	0.0830	6	-1.7505	1.8734	0.7405
log2D65_B	*HDAC3*	-0.3102	0.8520	0.9294	-0.1948	6	-2.3254	1.9824	0.8802
log2D65_B	*IL12a*	0.7459	0.2375	0.5182	1.3119	6	-0.5570	1.8448	0.4908
log2D65_B	*IL6*	-1.6488	0.0825	0.3298	-2.0824	6	-3.6448	0.2933	0.8047
log2D65_B	*IRAK4*	-0.9232	0.3676	0.6301	-0.9742	6	-2.2093	0.9510	0.6458
log2D65_B	*JNK1*	-0.9708	0.2905	0.5810	-1.1590	6	-2.2177	0.7921	0.6150
log2D65_B	*KI67*	-0.8018	0.9245	0.9365	-0.0988	6	-4.3050	3.9709	1.6911
log2D65_B	*MMP9*	-0.3770	0.5712	0.7695	-0.5988	6	-2.1473	1.3030	0.7050
log2D65_B	*MyD88*	-0.6818	0.0517	0.2481	-2.4225	6	-1.4503	0.0073	0.2978
log2D65_B	*NEMO*	-0.8354	0.5929	0.7695	-0.5645	6	-2.4891	1.5559	0.8266
log2D65_B	*OAZ1*	-0.5399	0.3151	0.5816	-1.0961	6	-1.6963	0.6467	0.4788
log2D65_B	*p38 (MAPK14)*	-1.1220	0.1179	0.4041	-1.8246	6	-2.4299	0.3540	0.5689
log2D65_B	*P50*	-1.0154	0.1982	0.5182	-1.4465	6	-2.1598	0.5549	0.5547
log2D65_B	*p65 (RELA)*	-0.3626	0.7044	0.8050	-0.3980	6	-1.8176	1.3090	0.6389
log2D65_B	*POLR2A*	-0.5472	0.4717	0.7547	-0.7678	6	-1.6513	0.8625	0.5137
log2D65_B	*SDHA*	-0.5912	0.6092	0.7695	-0.5391	6	-2.0344	1.2998	0.6813
log2D65_B	*TLR2*	-0.9164	0.0034	0.0408	-4.6790	6	-1.4310	-0.4483	0.2008
log2D65_B	*TLR6*	-1.1872	0.0016	0.0384	-5.4419	6	-1.7480	-0.6636	0.2216
log2D65_B	*TNF*	-1.1029	0.0241	0.1928	-2.9971	6	-1.9667	-0.1988	0.3613
log2D65_B	*TRAF6*	-0.9266	0.1980	0.5182	-1.4472	6	-1.9786	0.5080	0.5081
log2D65_B	*UBB*	0.1980	0.6938	0.8050	0.4133	6	-1.5430	2.1701	0.7587

Table S3. Statistical approaches applied in this study.

Figure	Test(s)	Notes	Mixed-Effects Model Specific Parameters			
			Baseline as fixed additive effect	**Time**	**Bayesian approach**	**Rescale**
1 A-C	Log-rank test	pairwise tests			NA	
1 D-E	Linear mixed-effects model	NA	No	Numbers	No	No
1 F-G	three-way ANOVA and pairwise *t* test	ANOVA with interaction term; *t* test for unpaired data			NA	
1 I-L	*t* test	unpaired data			NA	
2 A-E	Linear mixed-effects model	NA	Yes	Numbers	No	Yes, 2 B, D, E; No, others
2 F-I	Linear mixed-effects model	NA	Yes	Numbers	No	Yes, 2 I; No, others
2 J	Wilcoxon rank sum test	unpaired data			NA	
2 K	Ordinal logistic regression	NA			NA	
3 A-E Test 1	Linear mixed-effects model fit before and after the detected turning point	NA	Yes, before turning point; No, after turning point	Numbers	Yes, 3 A, B, C, and E before turning point, and 3 E after turning point; No, others	Yes, 3 D and E before and after the turning point; No, others
3 A-E Test 2	Wilcoxon rank sum test	performed for each time point or change between each of two time-points; unpaired data			NA	
3 G-K	Fisher's exact test	NA			NA	
4 B	two-way ANOVA and pairwise *t* test	ANOVA with interaction term; *t* test for unpaired data			NA	
4 C	three-way ANOVA and pairwise *t* test	ANOVA with interaction term; *t* test for unpaired data			NA	
4 D-I	*t* test	NanoString data DEG analysis: *t* test for unpaired data			NA	
S1 A-B	*t* test	*t* test on area under the curve for each treatment contrast			NA	

S2 C-J	Wilcoxon rank sum test	unpaired data,	NA			
S2 K-P	*t* test	unpaired data	NA			
S3 A	*t* test	*t* test on areas under the curve for each treatment contrast	NA			
S3 B-C	Wilcoxon rank sum test	unpaired data	NA			
S3 D-I and K	Linear mixed-effects model	NA	Yes	Numbers	Yes, S3 E, I; No, others	Yes, S3 D, E, H; No, others
S3 J	Linear mixed-effects model	NA	Yes	Factors	Yes	No
S4 A	Linear mixed-effects model	NA	No	Numbers	No	No
S4 B-F	Linear mixed-effects model	NA	Yes	Numbers	No	Yes
S4 G-L	Linear mixed-effects model fit before and after the detected turning point	NA	Yes, before turning point; No, after turning point	Numbers	Yes, S4 G and H before turning point, and S4 K before and after turning point; No, others	Yes, S4 J before and after turning point; No, others
S5	Linear mixed-effects model	NA	No	Factors	No	No
S6 C-I	Wilcoxon rank sum test	performed for each time point or change between each two time-points; unpaired data	NA			
S7 B-C	two-way ANOVA and pairwise *t* test	ANOVA with interaction term; *t* test for unpaired data	NA			

Supplementary References

1. H. Guo *et al.*, Multi-omics analyses of radiation survivors identify radioprotective microbes and metabolites. *Science* **370** (2020).
2. A. Chow *et al.*, Bone marrow CD169+ macrophages promote the retention of hematopoietic stem and progenitor cells in the mesenchymal stem cell niche. *The Journal of experimental medicine* **208**, 261-271 (2011).
3. I. Messaoudi, R. Estep, B. Robinson, S. W. Wong, Nonhuman primate models of human immunology. *Antioxid Redox Signal* **14**, 261-273 (2011).
4. P. Autissier, C. Soulas, T. H. Burdo, K. C. Williams, Immunophenotyping of lymphocyte, monocyte and dendritic cell subsets in normal rhesus macaques by 12-color flow cytometry: clarification on DC heterogeneity. *Journal of immunological methods* **360**, 119-128 (2010).
5. F. E. Grubbs, Procedures for detecting outlying observations in samples. *Technometrics* **11**, 1-21 (1969).
6. R Core Team, (2022) R: A language and environment for statistical computing. (version 2022). R Foundation for Statistical Computing, Vienna, Austria. https://www.R-project.org/
7. T. M. Therneau, P. M. Grambsh, *Modeling Survival Data: Extending the Cox Model* (Springer, New York, 2000).
8. B. L. Welch, The generalisation of student's problems when several different population variances are involved. *Biometrika* **34**, 28-35 (1947).
9. F. Wilcoxon, Individual Comparisons by Ranking Methods. *Biometrics Bulletin* **1**, 80-83 (1945).
10. J. M. Chambers, A. Freeny, R. M. Heiberger, "Analysis of variance; designed experiments" in Statistical Models in S (Wadsworth & Brooks/Cole, 1992), chap. 5.
11. D. Bates, M. Machler, B. Bolker, S. Walker, Fitting Linear Mixed-Effects Models Using lme4. *Journal of Statistical Software* **67**, 1-48 (2015).
12. Y. Chung, S. Rabe-Hesketh, V. Dorie, A. Gelman, J. Liu, A nondegenerate penalized likelihood estimator for variance parameters in multilevel models. *Psychometrika* **78**, 685-709 (2013).

13. F. Ibanez, Sur une nouvelle application de la theorie de l'information a la description des series chronologiques planctoniques. *J. Exp. Mar. Biol. Ecol.* **4**, 619-632 (1982).
14. M. G. Kendall, in *Time-series*. (Charles Griffin & Company, London, England, 1976).
15. G. E. P. Box, D. R. Cox, An Analysis of Transformations. *J. Roy. Stat. Soc. B.* **26**, 211-252 (1964).
16. W. N. Venables, B. D. Ripley, *Modern Applied Statistics with S*, 4th edition (Springer, New York, 2003).
17. S. S. Mangiafico, An R Companion for the Handbook of Biological Statistics, version 1.3.4. (2015).
18. J. Fox, S. Weisberg, *An R Companion to Applied Regression*, 3rd edition (SAGE Publications Inc., 2019).
19. A. Kuznetsova, P. B. Brockhoff, R. H. B. Christensen, lmerTest Package: Tests in Linear Mixed Effects Models. *Journal of Statistical Software* **82**, 1 - 26 (2017).
20. R. A. Fisher, *Statistical Methods for Research Workers*. S. J. Kotz, N.L., Ed., Series in Statistics (Springer, New York, 1992).
21. NanoString Technologies Inc., (2022) nCounter® Analysis System Grant Application Package [Brochure]. Nanostring Technologies. https://nanostring.com/wp-content/uploads/2023/03/BR_MK4429_nCounter_Brochure_r10.pdf.
22. Y. Benjamini, Y. Hochberg, Controlling the false discovery rate: a practical and powerful approach to multiple testing. *J. Roy. Stat. Soc. B.* **57**, 289-300 (1995).